

## Phase resolved deadtime of the Crab pulsar using IXPE data

M. VIVEKANAND<sup>1</sup>

<sup>1</sup>No. 24, NTI Layout 1<sup>st</sup> Stage, 3<sup>rd</sup> Main, 1<sup>st</sup> Cross, Nagasettyhalli, Bangalore 560094, India.

### ABSTRACT

After receiving an X-ray photon, an X-ray detector is not operational for a duration known as deadtime. It is detector specific and its effect on the data depends upon the luminosity of the source. It reduces the observed photon count rate in comparison to the expected one. In periodic sources such as the Crab pulsar, it can distort the folded light curve (FLC). An undistorted FLC of the Crab pulsar is required in combination with its polarization properties for studying its X-ray emission mechanism. This work derives a simple formula for the distortion of the FLC of a pulsar caused by the detector deadtime, and validates it using Crab pulsar data from the X-ray observatories *NICER* and *NUSTAR*, which have very small and relatively large detector deadtimes respectively. Then it derives a method for correcting the distorted FLC of the Crab pulsar in *IXPE* data, which has intermediate detector deadtime. The formula is verified after addressing several technical issues. This work ends with a discussion of why an undistorted FLC is important for studying the formation of cusps in the FLC of the Crab pulsar.

*Keywords:* Stars: neutron – Stars: pulsars: general – Stars: pulsars: individual PSR J0534+2200 – Stars: pulsars: individual PSR B0531+21 – X-rays: general

### 1. INTRODUCTION

X-ray detectors have a duration known as the detector deadtime which occurs after reception of an X-ray photon, during which they are inoperative. If the detector deadtime is much smaller than the mean time interval between X-ray photons from the source, which is the inverse of its expected count rate, then the observed count rate is also the same. As this mean time interval decreases in comparison to the detector deadtime, i.e. for more luminous sources, the ratio of the observed to the expected count rate decreases. The observed count rate is defined as the ratio of the observed number of X-ray photons  $N_o$  and the duration  $\Delta T$  in which they are observed. Now  $\Delta T$  is the sum of the durations  $\Delta T_d$  and  $\Delta T_l$ , which are the cumulative sub-durations in  $\Delta T$  in which the detector is dead and live, respectively. The expected count rate is the ratio  $N_o/\Delta T_l$ , since  $\Delta T_l$  is the actual time spent observing the source. This is larger than the observed count rate  $N_o/\Delta T$ .

For periodic sources such as the Crab pulsar, the folded light curve (FLC) is obtained by estimating the

phase (within the period) of each X-ray photon and forming a histogram of counts as a function of phase. For such sources  $\Delta T_d$  within a phase bin depends not only upon the expected count rate in that bin, but also that in several earlier phase bins, depending upon the relative values of the detector deadtime and the width of the phase bin. This can distort the observed FLC, which can be corrected by estimating  $\Delta T_d$  as a function of phase, also known as phase resolved deadtime.

Consider the deadtime of the the Neutron Star Interior Composition Explorer (*NICER*) satellite observatory (Gendreau & Arzoumanian 2018). *NICER*'s design makes its deadtime extremely low; the top panel of Fig. 1 shows the histogram of the deadtimes of a typical detector of *NICER*. About 87.34% and 7.07% of the deadtimes lie around the values 22.65 and 15.15  $\mu$  sec, respectively (LaMarr et al 2016; Stevens et al 2018; Vivekanand 2020); these two have not been shown in the figure, which shows the distribution of the rest. This results in a mean detector deadtime of  $23.1 \pm 4.2$   $\mu$  sec (Vivekanand 2020). For an average count rate of 211.3 counts per sec per detector, the mean time interval between photons is about 4.7 msec (Vivekanand 2020). Clearly this is a case of the detector deadtime being much smaller than the mean time interval between X-ray

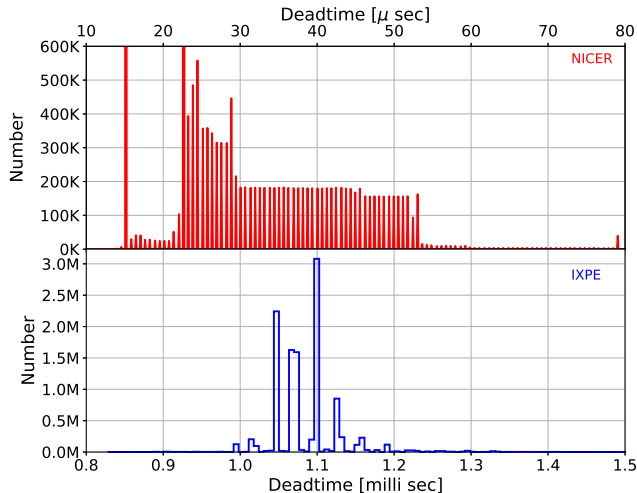


**Figure 1.** Top panel: Histogram of deadtimes for a typical detector of the *NICER* X-ray observatory for ObsID 1013010147. Abscissa is in micro seconds ( $\mu$  sec), the ordinate is in units of thousand counts, and the bin width is  $0.1 \mu$  sec. The bins at abscissa 22.65 and  $15.15 \mu$  sec have 176, 791, 344 and 14, 306, 804 counts respectively. Bottom panel: Histogram of deadtimes for detector DU1 of the ObsID 02001099 of the *IXPE* X-ray observatory. Abscissa is in milli seconds (msec), the ordinate is in units of million counts, and the bin width is  $7.2 \mu$  sec.

photons from the source; Fig. 8 of Vivekanand (2021) shows that the deadtime fraction is almost a replica of the expected light curve, and of a very small value, so the distortion of FLC is negligible.

Next consider The Nuclear Spectroscopic Telescope Array (*NuSTAR*) X-ray observatory (Harrison et al. 2013). It has two detectors (Focal Plane Detector Modules) each of which has a deadtime of 2.5 msec on account of event readout (Harrison et al. 2013; Madsen et al. 2015). The average count rate per module for the Crab pulsar is 250 counts /sec (Madsen et al. 2015) so the mean time between photons is 4 msec. Now the detector deadtime is relatively more comparable with the mean time interval between photons than in the *NICER* case. Further it is comparable to the width of the first peak of the FLC of the Crab pulsar. Therefore significant distortion of the FLC is expected; indeed the observed FLC in the top panel of Fig. 3 of Madsen et al. (2015) is a very distorted version of the corrected (expected) FLC shown in the second panel of the same figure.

Finally, consider the deadtime of one of the three detectors of the Imaging X-ray Polarimeter Explorer (*IXPE*) (Weisskopf et al 2022); the bottom panel of Fig. 1 shows the histogram of the deadtimes of detector DU1 of *IXPE*. The mean deadtime is  $1.088 \pm 0.071$

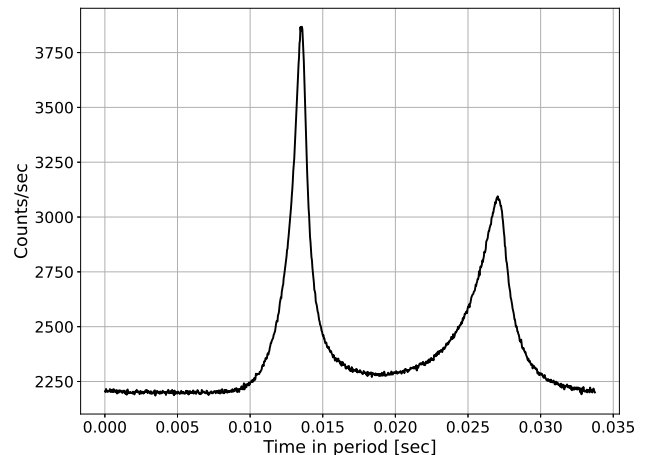


**Figure 2.** Expected (i.e., deadtime corrected) FLC of the Crab pulsar using *NICER* data of ObsIDs 1013010125, 1013010126, 1013010146, 1013010147, 1013010148, and 1013010150, in the energy range 2 – 8 keV. The abscissa has 1024 time bins in the average period  $P$  of these data ( $P = 1/29.626728$  sec).

msec<sup>1</sup>. The mean countrate for this observation is  $\approx 75.3$  counts per sec over its entire energy band, implying a mean time interval between X-ray photons of  $\approx 13.28$  msec. So this case is intermediate between the above two cases.

This work focuses on obtaining the phase resolved deadtime correction to the Crab pulsar’s FLC obtained from *IXPE* data. First, a simple analytical formula is derived that connects the observed and expected FLCs. This formula is verified using the first two cases. Then a method is given for obtaining the phase resolved deadtime correction for the *IXPE* data of the Crab pulsar, and then the results are verified as above. Finally, the importance of the phase resolved deadtime correction is discussed in connection with the X-ray emission mechanism of the Crab pulsar.

## 2. ANALYTIC FORMULA FOR PHASE RESOLVED DEADTIME

Let  $l_e(t)$  be the expected FLC of a pulsar which is a function of the time  $t$  within the pulsar period  $P$ ; over a duration of observation longer than  $P$ ,  $t \equiv t$  modulo  $P$ . The time  $t$  ranging from 0 to  $P$  is equivalent to the phase of the periodic signal ranging from 0 to 360 degrees. Let  $l_o(t)$  be the observed FLC. For reference the 2 – 8 keV  $l_e(t)$  of the Crab pulsar from the *NICER* data of the six

<sup>1</sup> <https://heasarc.gsfc.nasa.gov/docs/ixpe/analysis/IXPE-SOC-DOC-008A.L>

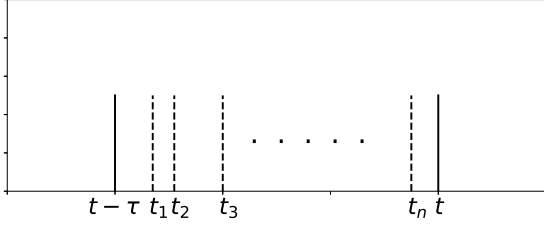


**Figure 3.** Arrival times  $t_1, t_2, t_3, \dots, t_n$  and  $t$  of  $n+1$  X-ray photons in the duration  $t - \tau$  to  $t$ . These are determined by the expected FLC  $l_e(t)$  and Poisson statistics. The photon at time  $t$  can be observed only if the  $n$  earlier photons were not received.

largest data files will be used, which is shown in Fig. 2; details of its estimation are given in Vivekanand (2020).

Now consider a small time interval  $\Delta t$  after a given time  $t$ . In an observation of total duration  $T_0$  sec, there are  $T_0/P$  periods, so the expected and observed number of photons in the time interval  $\Delta t$  are  $(l_e(t) \times \Delta t) \times (T_0/P)$  and  $(l_o(t) \times \Delta t) \times (T_0/P)$ , respectively. Let  $f_d(t)$  be the deadtime fraction per unit time at the time  $t$ . Then by definition,

$$l_o(t)\Delta t(T_0/P) = l_e(t)[\Delta t \times (1 - f_d(t))](T_0/P), \quad (1)$$

which implies that

$$\begin{aligned} l_e(t) &= l_o(t)/(1 - f_d(t)) \\ \Rightarrow f_d(t) &= 1 - l_o(t)/l_e(t). \end{aligned} \quad (2)$$

Thus one can obtain the expected FLC from the observed FLC and the deadtime fraction, both of which are observed quantities.

For further derivation the following assumptions are made: (1) the detector deadtime  $\tau$  is a constant; (2)  $\tau \ll P$ ; (3)  $l_e(t)$  and  $l_o(t)$  are well defined and  $> 0$ ; (4)  $T_{ph}$  is the mean time interval between two subsequent photons; the observed and expected  $T_{ph}$  are the inverse of the corresponding FLCs ( $1/l_o(t)$  and  $1/l_e(t)$ ).

Let  $P_e(t)$  be the expected normalized probability density of photon arrival at time  $t$ ; the actual probability of its arrival in a small time interval  $\epsilon$  is  $P_e(t) \times \epsilon$ . Clearly  $P_e(t)$  depends upon  $l_e(t)$ . Now, the observed normalized probability density  $P_o(t)$  depends not only upon  $P_e(t)\epsilon$  but also the probability that no photon arrives in the time duration  $t - \tau$  to  $t$ . This can be estimated by dividing this time duration  $\tau$  into  $M$  sub intervals of duration  $\epsilon$ , and taking the limits  $\epsilon \rightarrow 0$  and  $M = \tau/\epsilon$ . Figure 3 is a cartoon of the scenario being discussed here. Therefore the observed probability of receiving a photon in the duration  $\epsilon$  at time  $t$  is given by

$$P_o(t)\epsilon = P_e(t)\epsilon \times [1 - P_e(t - \epsilon)\epsilon] \times [1 - P_e(t - 2\epsilon)\epsilon]$$

$$\begin{aligned} &\times [1 - P_e(t - 3\epsilon)\epsilon] \dots \times [1 - P_e(t - M\epsilon)\epsilon] \\ &= P_e(t)\epsilon \prod_{i=1}^M [1 - P_e(t - i\epsilon)\epsilon] \\ &\approx P_e(t)\epsilon \left[ 1 - \sum_{i=1}^M P_e(t - i\epsilon)\epsilon \right] \\ &\approx P_e(t)\epsilon \left[ 1 - \int_{t-\tau}^t P_e(t)dt \right]. \end{aligned} \quad (3)$$

In eqn 3 only terms linear in  $\epsilon$  have been retained, and the summation has been converted into an integral.

Both  $P_e(t)$  and  $P_o(t)$  are defined above as being normalized. The common implication is that  $\int_0^P P_e(t)dt = 1$ . However in our context  $\int_0^P P_e(t)$  is equal to the average number of photons per period which is  $\int_0^P l_e(t)dt$ .

Now a model of  $P_e(t)$  is required to connect it to  $l_e(t)$ . We will make the simple assumption that the actual probability  $P_e(t)\epsilon \approx \epsilon/(\alpha \times T_{ph})$  where  $\alpha$  is a constant to be determined but which is expected to be close to  $\approx 1$ . This assumption makes logical sense, it is linearly proportional to  $\epsilon$ , and finally it helps in deriving the simple analytic formula below. But  $T_{ph} = 1/l_e(t)$ , so  $P_e(t) \approx l_e(t)/\alpha$ ; i.e., the expected probability density  $P_e(t)$  is linearly proportional to the expected FLC  $l_e(t)$ . The same argument can be extended to the observed probability density  $P_o(t)$ , so that

$$\begin{aligned} l_o(t) &= l_e(t) \times \left[ 1 - \int_{t-\tau}^t (l_e(t)/\alpha)dt \right] \\ \Rightarrow f_d(t) &= \int_{t-\tau}^t (l_e(t)/\alpha)dt. \end{aligned} \quad (4)$$

This is the simple formula that relates the observed and expected FLC at a given time to the phase resolved deadtime fraction.

One can make the model more sophisticated by using the known distribution of  $\tau$  instead of using a constant  $\tau$ . One can derive a more rigorous relation between  $P_e(t)$  and  $l_e(t)$  that may be non-linear, but that may not lead to the simple analytic formula of eqn 4. As shown later, this simple formula is sufficient for our purpose. The parameter  $\alpha \approx 1$  for the *NICER* and *IXPE* instruments, and needs to be set to  $\approx 2$  for *NuSTAR*, which has a significant distortion of  $l_e(t)$  due to  $\tau$ .

An interesting aspect of eq. 4 is that for peaks in  $l_e(t)$ , the corresponding peaks in  $f_d(t)$  are shifted towards larger times by the about  $\approx \tau/2$ . This can be understood by recognizing that the integral in eq. 4 is essentially a moving average filter. Now a conventional moving average filter would have an integral of the kind  $\int_{t-\tau/2}^{t+\tau/2} (l_e(t)/\alpha)dt$ , the limits of integration being from

$t - \tau/2$  to  $t + \tau/2$ , which is symmetric around  $t$ . However in eq. 4 the limits are asymmetric around  $t$ . It is easy to show therefore that if  $l_e(t)$  was a symmetric pulse, like a Gaussian, then eq. 4 would give a symmetric pulse shaped deadtime fraction  $f_d(t)$  whose peak is shifted by about  $\approx \tau/2$  for at least small  $\tau$ .

Equation 4 fails when the integral evaluates to  $> 1.0$  which makes the deadtime fraction  $f_d(t) > 1$ , and the observed FLC  $l_o(t)$  negative, both of which are unphysical. This occurs when either the deadtime  $\tau$  is large, or the expected FLC  $l_e(t)$  is large, or both.

### 2.1. Verification of formula using NICER data

For very small values of  $\tau$ , eqn 4 reduces to

$$\begin{aligned} f_d(t) &\approx \tau l_e(t) / \alpha \\ &\approx \tau l_e(t), \end{aligned} \quad (5)$$

if  $\alpha$  is assumed to be 1. Thus the deadtime fraction is linearly proportional to the expected FLC. This is clearly seen in Fig. 8 of Vivekanand (2021). The count rate at the first peak in the top panel of that figure is 318, so eqn 4 gives  $f_d(t) = 23.1 \times 318 / 1000000 = 0.73\%$ . The corresponding value in the bottom panel of that figure is 0.77%. The difference of  $\approx 0.04\%$  is due to the fact that the top panel of Fig. 8 of Vivekanand (2021) consists of X-ray photons only while the bottom panel has about  $\approx 8\%$  more counts that are not from the Crab pulsar but still contribute to the deadtime (Vivekanand 2021).

Similarly the count rate at the first sample in the top panel of that figure is 203, so  $f_d(t) = 23.1 \times 203 / 1000000 = 0.47\%$ . The corresponding value in the bottom panel of that figure is 0.50%, the difference once again being consistent with the additional  $\approx 8\%$  more counts contributing to the deadtime but not to the FLC.

In the *NICER* case the shift in the peak of  $f_d(t)$  is not noticeable because  $\tau$  is smaller than the bin width.

Thus the formula in eqn 4 has been verified for *NICER* data of the Crab pulsar.

### 2.2. Verification of formula using NuSTAR data

The ideal starting point for verifying eqn 4 is the actual expected FLC  $l_e(t)$  which is obviously not available; only the observed FLC  $l_o(t)$  is available. However for *NICER* data of the Crab pulsar the deadtime  $\tau$  is very small, so the difference between  $l_e(t)$  and  $l_o(t)$  is also very small. So in the previous sub-section we used the deadtime corrected  $l_o(t)$  as the actual  $l_e(t)$  for *NICER* data, shown in the top panel of Fig. 8 of Vivekanand (2021), which includes the entire energy range of the *NICER* observatory.

For this section also we ideally need to use the actual  $l_e(t)$  which is not available. Since  $\tau$  for *NuSTAR* data is quite large, significant differences are expected between  $l_o(t)$  and the actual  $l_e(t)$ . So we can not use the estimated  $l_e(t)$  given in the middle panel of Fig. 3 of (Madsen et al. 2015), to reproduce the  $l_o(t)$  in the top panel of that figure, using eqn 4 above. Therefore we can not do any quantitative comparison here. Therefore in this section we will use the  $l_e(t)$  in Fig. 2 above since only a qualitative comparison is attempted here. This figure was prepared for verification of the *IXPE* case which follows later. The use of Fig. 2 in this section is discussed in greater detail later on.

The mean X-ray flux of the Crab pulsar per detector of the *NuSTAR* observatory is  $\approx 250$  counts/sec (Madsen et al. 2015), while at the first peak it is  $\approx 400$  counts/sec. The corresponding observed  $T_{ph}$  are 4 and 2.5 msec respectively. This is a case of the detector deadtime (2.5 msec) being comparable to the  $T_{ph}$ . This reduces the accuracy of the formula in eqn 4. However the formula of eqn 4 does quite well with the *NuSTAR* data if  $\alpha$  is chosen to be  $\approx 2$  instead of 1; its implications will be discussed later on.

We start by assuming that the FLC in Fig. 2 is the actual  $l_e(t)$  for the *NuSTAR* data of the Crab pulsar if it is scaled to reflect the mean counts per sec. This data is smoothed by implementing a moving average filter over 5 samples to approximately reflect the number of samples per period in the top panel of Fig. 3 of Madsen et al. (2015). Then the data is scaled to give an average count rate of 250 counts/sec. Then eqn 4 is used with  $\tau = 2.5$  msec and  $\alpha = 2$  to obtain the observed FLC  $l_o(t)$ . This data is then passed through a box shaped low pass filter of time constant 3.4 msec to produce the damped oscillations observed by Madsen et al. (2015) in the top panel of their Fig. 3. The result is shown in Fig. 4, which compares very well with the corresponding curve in the top panel of Fig. 3 of Madsen et al. (2015).

With the peak in Fig. 4 normalized to the value 1.0, the first and second minima at  $t = 0.01567$  and  $t = 0.02932$  are 0.67 and 0.70 respectively; these are consistent with the values in the top panel of Fig. 3 of Madsen et al. (2015). The secondary maximum at  $t = 0.02649$  is 0.90, which is also consistent with the corresponding value in top panel of Fig. 3 of Madsen et al. (2015). The only difference is the damped oscillation before the first peak, which is missing in their Fig. 3; this difference is discussed in greater detail later on. Further, Madsen et al. (2015) note in the legend of their Fig. 3 that “the minimum of the live-time curve occurs just after the peak”, as expected from eqn 4, by an amount that they do not specify, but which appears to

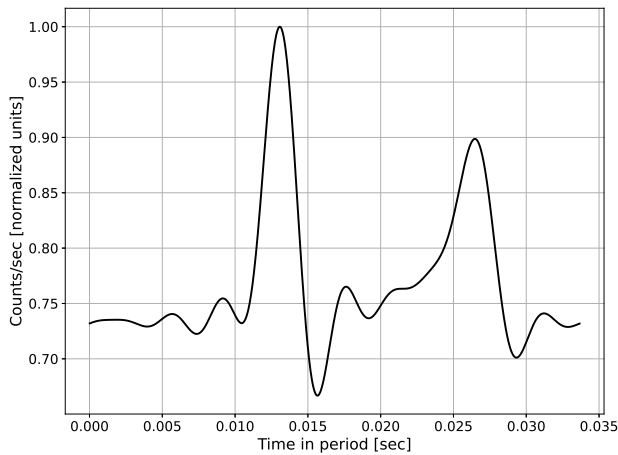


**Figure 4.** The FLC obtained by using eqn 4 on a scaled version of Fig. 2 and using a low pass filter of smoothing time 3.4 msec.

be at least 0.7 ms by visual analysis. While this is not entirely consistent with the expected value of  $2.5/2 = 1.25$  ms, it is in the correct ball park.

Thus Fig. 4 is a reasonable verification of eqn 4 for the Crab pulsar data of *NuSTAR* (assuming that  $\alpha = 2$ ), even though the deadtime  $\tau$  in this case is relatively large.

Figure 2 contains data in the energy range 2 to 8 keV while the energy range of *NuSTAR* is from 3 to 78 keV (Madsen et al. 2015). However the Crab pulsar has a very steep power law spectrum (Vivekanand 2021) so most of the photons in the FLC are at the lower energies. So we can ignore the spectral evolution of the Crab pulsar’s FLC for our qualitative analysis.

In section 2 we made the assumption that  $P_e(t)\epsilon \approx \epsilon/(\alpha \times T_{ph}) \approx \epsilon l_e(t)/\alpha$ . Since  $\tau$  is large in the *NuSTAR* case, the count rate of the actual light curve needs to be lowered by setting  $\alpha = 2$  to get sensible results. This can by no means be considered a rigorous “fix” of the formula, but Fig. 4 shows that this “fix” achieves quite accurate qualitative results. The ideal solution is to get a more accurate relation between  $P_e(t)$  and  $l_e(t)$ .

### 3. DEADTIME ESTIMATION FOR *IXPE*

A very brief introduction to *IXPE* is given in its quickstart guide<sup>2</sup>. More details are provided in its observatory<sup>3</sup> and instrument<sup>4</sup> guides.

For our purpose it is sufficient to know that there are three gas pixel detectors (GPD) each of which produces a track after absorbing an X-ray photon; this track contains information about the polarization of that photon. The deadtime of the detector depends upon the time required to read the electrons in this track; section 2.2 of the instrument guide discusses this in detail. An example of deadtime distribution is given in the bottom panel of Fig. 1. The deadtime is recorded in the level-1 data files of *IXPE* in terms of the parameter *LIVETIME*, which is the detector live time since the previous event. Let two successive events occur at the *IXPE* detector at times  $t_1$  and  $t_2$ , with *LIVETIME*s  $l_1$  and  $l_2$ , respectively. Then the deadtime after the first event is  $(t_2 - t_1) - l_2$ , since the interval between any two successive events is the sum of the deadtime after the first event and the live time until the next event.

However the events recorded in the level-2 files are often not successive, since this data has gone through several filters such as passage of the observatory through the South Atlantic Anomaly (SAA), entering Earth occultation, etc. Thus, the event-by-event *LIVETIME* becomes useless and can not be carried forward to level-2 files. So eqn. 4 is applicable to data in the level-1 files only, which include all events, since “Level-1 Science Event data contain the same information as Level-0 Science Event data but converted to FITS format”<sup>5</sup>. Therefore in this section the *IXPE* level-2 data files are used for obtaining the observed FLC while the corresponding level-1 data files are used to derive the phase resolved deadtime fraction. Note that the level-1 files probably can not be used to obtain the observed FLC since these contain events that are not related to the X-ray source but nevertheless contribute to the detector deadtime. Further, both level-1 and level-2 data files have to be referred to the barycenter frame for phase resolved analysis.

Currently data of three ObsIDs are available for *IXPE* – 01001099, 02001099 and 02006001. Data of ObsID 01001099 has problems described by Bucciantini et al (2023) with details in the README file associated with this paper. ObsID 02006001 has  $\approx 2.5$  times less data than ObsID 02001099, so only the latter has been considered for analysis in this section. The average count rate per *IXPE* detector for the Crab pulsar is  $\approx 44$  counts/sec in the energy range 2 to 8 keV, but differs slightly from detector to detector.

The algorithm for the analysis of this section is the following:

<sup>2</sup> [https://heasarc.gsfc.nasa.gov/docs/ixpe/analysis/ixpe\\_quickstart\\_v2.pdf](https://heasarc.gsfc.nasa.gov/docs/ixpe/analysis/ixpe_quickstart_v2.pdf)

<sup>3</sup> [https://heasarc.gsfc.nasa.gov/docs/ixpe/analysis/IXPE-SOC-DOC-0115A\\_UG-Observatory.pdf](https://heasarc.gsfc.nasa.gov/docs/ixpe/analysis/IXPE-SOC-DOC-0115A_UG-Observatory.pdf)

<sup>4</sup> [https://heasarc.gsfc.nasa.gov/docs/ixpe/analysis/IXPE-SOC-DOC-007D\\_UG-Instrument.pdf](https://heasarc.gsfc.nasa.gov/docs/ixpe/analysis/IXPE-SOC-DOC-007D_UG-Instrument.pdf)

<sup>5</sup> [https://heasarc.gsfc.nasa.gov/docs/ixpe/analysis/IXPE-SOC-DOC-007D\\_UG-Instrument.pdf](https://heasarc.gsfc.nasa.gov/docs/ixpe/analysis/IXPE-SOC-DOC-007D_UG-Instrument.pdf)



**Table 1.** Crab pulsar’s rotation parameters for obtaining the observed FLC from the data of OBS\_ID 02001099.

Parameter	Value
Epoch (MJD)	60017.226732
$\nu_0$ (Hz)	29.5746291403(9)
$\dot{\nu}_0$ ( $10^{-10}$ Hz s $^{-1}$ )	-3.67074(1)
$\ddot{\nu}_0$ ( $10^{-21}$ Hz s $^{-2}$ )	8.5(2)

1. There is a level-2 data file for each of the three detectors. Barycenter these epochs, combine them and obtain the best fit rotation frequency  $\nu_0$  of the Crab pulsar and its first and second derivatives  $\dot{\nu}_0$  and  $\ddot{\nu}_0$  using the stride-fit method (Vivekanand 2020). The second derivative is required since this data duration is more than 40 days. The results are shown in Table 1. Further analysis has to be done separately for each detector.
2. For each detector there are two level-1 files. For each of them, there are two Good Time Interval (GTI) extensions. These two GTIs are merged with the GTI of the corresponding level-2 data file using the AND mode, i.e., output GTI contains time intervals common to the three input GTI (also known as the intersection set). Note that the second GTI extension has an extra column named RUN\_ID which should be deleted beforehand.
3. Then the level-1 data files are filtered using the merged GTI extension. Sequential pairs of the TIME and LIVETIME values are processed to yield three epochs, viz., the epoch of the current event, this epoch plus the deadtime, and the epoch of the next event, the condition being that the pair must belong to the same GTI.
4. Finally these three epochs are referred to the barycenter.

The result of the above algorithm is that one has two output files for each of the three detectors, each file containing three columns of barycentered times – the epoch of an event, the epoch of the next sequential event, and an intervening epoch signifying the end of the deadtime after the first event, or equivalently the start of the livetime before the next sequential event. Clearly the difference between the times of the intervening and first events is the deadtime at that epoch, while the difference between the times of the third and intervening events is the corresponding livetime. By estimating the phase within the Crab pulsar period of the first event, one can make a histogram of the deadtime and livetime as a

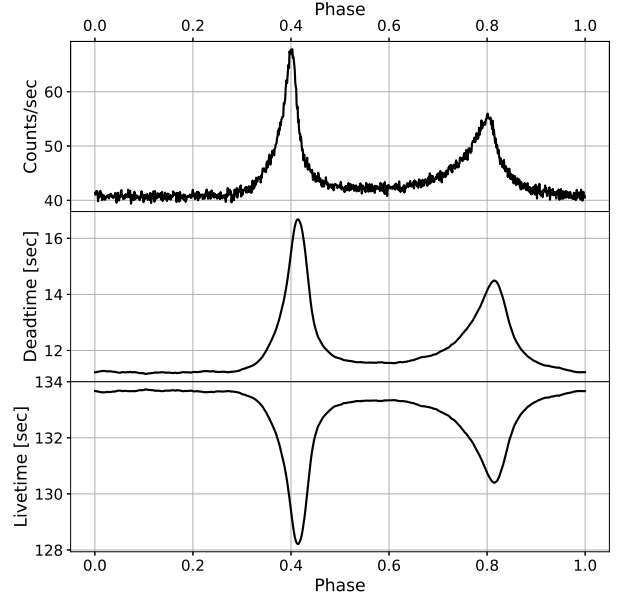


**Figure 5.** Top panel: Observed FLC of the Crab pulsar in the energy range 2 – 8 keV from Detector 1 of ObsID 02001099 of *IXPE* level-2 data. Middle panel: Phase resolved deadtime of the same detector from level-1 data. Bottom panel: Phase resolved livetime of the same detector from level-1 data.

function of phase within the period; this has been done for *NuSTAR* by Madsen et al. (2015) and for *NICER* by Vivekanand (2020, 2021).

Figure 5 shows the result of applying this algorithm on the data of detector DU1 of ObsID 02001099 of *IXPE* data. The top panel shows the observed FLC of the Crab pulsar using the level-2 data, while the middle and bottom panels show the phase resolved deadtime and livetime, respectively, estimated from the level-1 data. The peak of the deadtime is shifted by about  $1.088/1000/2 * 29.626728 \approx 0.016$  in phase with respect to the peak of the FLC, as expected from eqn 4. The deadtime and livetime are perfectly anti correlated as expected, since their sum is the total time spent observing the source at that phase; this quantity is independent of phase, its average value per phase bin being  $144.9 \pm 0.3$  sec.

The phase resolved deadtime fraction (observed) can be obtained from Fig. 5 by the formula  $f_d(t) = \text{deadtime} / (\text{deadtime} + \text{livetime})$ . The minimum, maximum and mean values of the deadtime fraction are 7.70% (per cent), 11.51% and 8.29% respectively; the error on these quantities is  $\approx 0.02\%$ . Bucciantini et al (2023) mention that the difference between the maximum and minimum deadtime fractions “is estimated to be less than 3%”;

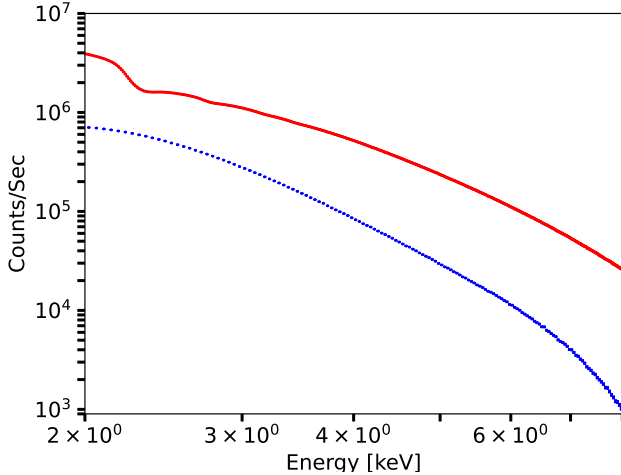


**Figure 6.** Raw spectrum of the Crab pulsar in the energy range 2 to 8 keV using the *NICER* (red curve) and *IXPE* (blue curve) data.

the corresponding number here is  $11.51 - 7.70 = 3.81\%$ . Thus the result of [Bucciantini et al \(2023\)](#) can be considered to be preliminary but in the right ball park, and any further study requires a more rigorous calculation.

Now we need to use eqn. 4 on the actual  $l_e(t)$  of *IXPE* data to estimate the expected  $f_d(t)$ . However this is not available. So we instead use the FLC in Fig. 2 which pertains to the *NICER* data in the same energy range as *IXPE*. Now the FLC of the crab pulsar evolves with energy. Figure 6 shows the raw spectrum of the *NICER* and *IXPE* data in the same energy range; the spectra are roughly of the same shape in this energy range, but some differences exist between them, which will be discussed later on. So we will go ahead and use Fig. 2 as the actual  $l_e(t)$  for this section.

From Fig. 5 the observed  $f_d(t)$  should be compared with the expected  $f_d(t)$  obtained by using eqn. 4 (with  $\alpha = 1$ ) on the data of Fig. 2, after scaling for the mean count rate of  $\approx 44/(1 - 0.083) \approx 48$  photons/sec for a single detector. A direct comparison of these two curves proves difficult because the Crab nebula background counts are significantly different in the *NICER* and *IXPE* cases. So the nebular background was estimated in both  $f_d(t)$  curves by estimating the mean value of the counts in the off-pulse phases (0.0 to 0.2). After subtraction of the nebular background the area under each  $f_d(t)$  curve was normalized to the value 1.0. These two curves are shown in the top two panels of Fig. 7; the bottom panel shows their difference.

We identify three phase regions for comparison – region 1 being under the first peak, extending from phase 0.35 to 0.45, region 2 being under the second peak, ex-

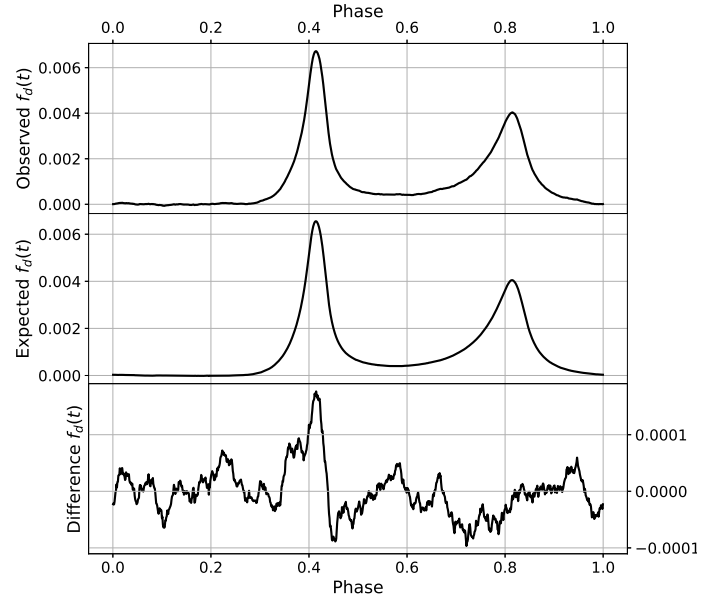


**Figure 7.** Top panel: Observed  $f_d(t)$  derived from the second and third panels of Fig. 5, after removing the off-pulse mean and normalizing the area under the curve to 1.0. Middle panel: Expected  $f_d(t)$  estimated using eqn. 4 on the data of Fig. 2, after mean removal and area normalization. Bottom panel: the difference between the top and middle panels.

tending from phase 0.75 to 0.85, and region 3 being the rest of the phases. The mean and standard deviation of the difference curve in region 3 are  $-5.7 \times 10^{-6}$  and  $31.5 \times 10^{-6}$  respectively. Using these values the  $\chi^2$  per degree of freedom in the three regions are 10.6, 1.1 and 1.0 respectively. The reduced  $\chi^2$  is 1 for region 3 as expected, and is close to 1 under the second peak, but significantly higher than the expected value of  $\approx 1$  under the first peak.

The difference under the first peak could be due to two factors – lack of alignment of the observed and expected  $f_d(t)$  curves at the level of fraction of a phase bin, which would result in a sharp rise and fall of the difference curve under the first peak; or energy evolution of the FLC due to the slightly differing raw spectra in Fig. 6. To test the first hypothesis, one of the curves was shifted with respect to the other by various fractions of the bin width, using Fourier techniques, but no improvement was noticed. This leaves the second possibility, that our choice of Fig. 2 for the actual  $l_e(t)$  of *IXPE* is not completely valid.

There might also be issues related to alignment of the curves because of insufficient number of photons in the FLC of the *IXPE* data, which was aligned with the FLC

of *NICER* data in Fig. 2. Attempt to align the two curves showed that the mis-alignment is smaller than the bin width of the data. Thus the alignment can be improved only by obtaining more *IXPE* data of longer observations on the Crab pulsar. In fact it is for this very reason that data of the third ObsID (02006001) could not be used, since its data was too meager for FLC alignment.

The qualitative nature of the difference  $f_d(t)$  for the other two detectors (DU2 and DU3) of *IXPE* is similar to that of detector DU1, the sharp swing under the peak being prominent. For DU2 the  $\chi^2$  per degree of freedom in the three regions are 13.3, 2.2 and 1.0; for DU3 the values are 24.9, 2.8 and 1.0.

While the  $\chi^2$  give one kind of information, it can be noticed that the maximum departure of the difference curve in region 1 is  $0.00017/0.00658 = 0.026$ , which is not too different from the Poisson error due to photon counts of  $\approx 0.01$  at the peak of the FLC. So the analysis of this section may be facing problems of both energy evolution of the FLC, and low photon counts.

Thus Fig. 7 is a reasonable verification of eqn 4 for the Crab pulsar data of *IXPE* (assuming that  $\alpha = 1$ ).

#### 4. DISCUSSION

Finally, the corrected FLC for each detector is obtained by using the observed deadtime fraction  $f_d(t)$  and the observed FLC in eqn. 2. This has to be done separately for each detector since there can be minor differences between the parameters of each detector. For example, the average deadtimes for the three detectors are  $1.088 \pm 0.071$  msec,  $1.096 \pm 0.074$  msec, and  $1.094 \pm 0.074$  msec, which are almost the same. However their mean count rates are  $75.25 \pm 0.02$ ,  $70.66 \pm 0.02$  and  $67.76 \pm 0.02$  respectively. their maximum difference is  $(75.25 - 67.76)/75.25 \approx 10\%$ , which is not insignificant in our context since the observed FLC  $l_o(t)$  in eqn. 2 would be proportional to these values.

A critical assumption in the above analysis is that one is processing pairs of successive events. However this is not guaranteed; some events may be missing or filtered out for various reasons. Thus if one had three successive events at times  $t_1$ ,  $t_2$  and  $t_3$ , with LIVETIMES  $l_1$ ,  $l_2$  and  $l_3$  respectively, and if the intervening event was missing, one would be processing events  $t_1$  and  $t_3$ , and the derived deadtime and livetime for this pair would be in error, depending upon what values were recorded as LIVETIME. The maximum deadtimes estimated for each detector are 7.367, 7.806 and 7.421 msec respectively; clearly these extreme values are not part of statistical distributions whose mean value is  $\approx 1.09$  msec with standard deviation of  $\approx 0.07$  msec. Therefore it

is possible that some of these extreme values could be erroneous deadtime estimates. However the number of these extreme deadtime values is insignificant, as seen in the lower panel of Fig. 1.

The average livetimes of the three detectors are 12.043, 12.886 and 13.480 msec; their inverses are 83.04, 77.60 and 74.18 counts/sec respectively. These differ from the observed count rates above by the expected correction for the deadtime, as expected. The maximum livetime values estimated for the three detectors are 180.682, 217.177, and 231.013 msec respectively. Once again some of these extreme livetime estimates may be fake, because it is unlikely that no photons are detected by the DU in a duration of  $\approx 200$  msec when the mean time between photons is expected to be  $\approx 12$  to 13 msec.

Attempt was made to suppress the damped oscillation before the first peak in Fig. 4, to be consistent with the top panel of Fig. 3 of Madsen et al. (2015). Various integration times were used in eqn. 4 along with different filter time constants, but the damped oscillations behaved similarly at both peaks; it was not possible to suppress only one of them. So it is possible that some other physical effect is operative here.

The dependence of deadtime upon photon energy was tested by plotting LIVETIME against the level-1 equivalent of photon energy PHA and PHA\_EQ. Scatter plots were made between PHA and PHA\_EQ, and PHA and LIVETIME. The former pair of parameters were highly correlated for each detector as expected, since they are essentially the same quantity. The latter pair showed no correlation, even when the LIVETIME at an epoch was correlated with the PHA of the epoch just before that. It is therefore concluded that there is no energy dependence of the deadtime. However this could also arise due to the fact that spectrum is dominated by photons in a narrow energy range of 2 – 4 keV, and also possible by the poor photon statistics.

##### 4.1. X-ray emission mechanism of the Crab pulsar

The characteristic feature of the Crab pulsar's X-ray FLC (Fig. 2) is its first peak, also known as the main pulse. This luminous and narrow peak is believed to be due to the formation of caustics in the high energy emission region of the Crab pulsar. Caustics are formed when photons from different regions of the pulsar magnetosphere arrive at the same time at the observer, which is believed to be due to a combination of special relativistic aberration and light travel time (see Romani & Yadigaroglu (1995), Bai & Spitkovsky (2010) and Harding (2016) and references therein).



Romani & Yadigaroglu (1995) reproduce the fast sweep of the position angle of linear polarization of the Crab pulsar in relation to its first peak in the FLC (see their Fig. 5), and it is consistent with the optical polarization data of the Crab pulsar of (Smith et al 1988) and Słowikowska et al (2009). Both works show that the percentage of linear polarization of the Crab pulsar at optical wavelengths is not minimum under the first peak of optical FLC, but is situated a bit beyond it in phase. In fact Słowikowska et al (2009) state that it is minimum at the peak of the radio FLC.

To study the X-ray emission mechanism of the Crab pulsar one needs both an X-ray FLC and phase resolved X-ray polarization data with sufficient signal to noise ratio and high phase resolution ( $\geq 1024$  bins in the period); *IXPE* is capable of providing such data. If caustics form in the Crab pulsar's FLC as postulated, then a sharp peak in the FLC is expected where photons from different regions of the magnetosphere arrive at the same time at the observer. By the same token,

the percentage of linear polarization should decrease under the sharp peak, since photons from different regions of the magnetosphere will have differing position angles of linear polarization, depending upon the geometry of the magnetic field and the specific high energy emission mechanism. This difference, between the phase of the maximum of the first peak of the X-ray FLC and the phase of the minimum of the percentage of X-ray linear polarization, may be an important constraint for the X-ray emission mechanism of the Crab pulsar. Correcting the observed X-ray FLC using the observed deadtime fraction  $f_d(t)$  is an important step in this direction.

This work has made use of the publicly available data from the *NICER* and *IXPE* X-ray observatories.

I thank the *IXPE* helpdesk for discussion regarding the instrumental issues of this work. I thank Niccolo Bucciantini and the referee for helpful comments.

## REFERENCES

- Bai, X.N., Spitkovsky, A., 2010, *ApJ*, 715, 1270  
 Bucciantini, N. Ferrazzoli, R., Bachetti, M. et al 2023, *NatAs*, 7, 602  
 Gendreau, K. & Arzoumanian, Z. 2017, *NatAs*, 1, 895  
 Harding, A. 2016, *J. Plasma Phys.* 82, 635820306  
 Harrison, F.A., Craig, W. W., Christensen, F. E., et al. 2013 *ApJ*770, 103  
 LaMarr, B., Prigozhin, G., Remillard, R., et al 2016, *Proc. SPIE*, 9905, 99054W  
 Madsen, K. K., Reynolds, S., Harrison, F., et al. 2015, *ApJ*, 801, 66  
 Romani, R.W. & Yadigaroglu, I.A. 1995, *ApJ*, 438, 314  
 Słowikowska, A., Kanbach, G., Kramer, M., et al 2009, *MNRAS*, 397, 103  
 Smith, F.G., Jones, D.H.P., Dick, J.S.B., et al 1988, *MNRAS*, 233, 305  
 Stevens, A.L., Uttley, P., Altamirano, D., et al 2018, *ApJL*, 865, L15  
 Vivekanand, M. 2020, *A&A*, 633, A57  
 Vivekanand, M. 2021, *A&A*, 649, A140  
 Weisskopf, M. C., Soffitta, P., Baldini, L. et al 2022, *Journal of Astronomical Telescopes, Instruments, and Systems*, Vol. 8, No. 2, article id. 026002